PAPER

Incommensurate magnetic ordering in CrB$_2$

View the article online for updates and enhancements.

Incommensurate magnetic ordering in CrB$_2$

A Deák[1] , **J Jackson**[2] , **B Nyári**[1,3,*] **and L Szunyogh**[1,3]

[1] Department of Theoretical Physics, Institute of Physics, Budapest University of Technology and Economics, Műegyetem rkp. 3, H-1111 Budapest, Hungary
[2] STFC Scientific Computing Department, Daresbury Laboratory, WA4 4AD Warrington, United Kingdom
[3] ELKH-BME Condensed Matter Research Group, Budapest University of Technology and Economics, Műegyetem rkp. 3, H-1111 Budapest, Hungary

E-mail: nyari.bendeguz@ttk.bme.hu

CrossMark

Abstract

Incommensurate magnetism in CrB$_2$ is studied in terms of a spin model based on density functional theory calculations. Heisenberg exchange interactions derived from the paramagnetic phase using the disordered local moment (DLM) theory show significant differences compared with those resulting from the treatment of the material as a ferromagnet; of these two methods, the DLM theory is found to give a significantly more realistic description. We calculate strongly ferromagnetic interactions between Cr planes but largely frustrated interactions within Cr planes. Although we find that the ground state ordering vector is sensitive to exchange interactions over a large number of neighbour shells, the q-vector of the incommensurate spin spiral state is satisfactorily reproduced by the theory (0.213 compared with the known ordering vector $0.285 \times (2\pi)/(a/2)$ along Γ–K). The strong geometric frustration of the exchange interactions causes a rather low Néel temperature (about 97 K), also in good agreement with experiment.

Keywords: incommensurate spin spiral, disordered local moment, *ab initio*, frustration, Heisenberg exchange

(Some figures may appear in colour only in the online journal)

1. Introduction

Beside geometric frustration stemming from an incompatibility of the underlying lattice with magnetic interactions, frustration caused by competing exchange couplings is also known to lead to non-collinear magnetic ordering. Not only can it cause spin spiral ground states in atomic chains [1, 2] and surfaces [3], it can also contribute to the stabilization of skyrmions [4, 5] and induce an effective attractive interaction between them [6]. Frustrated interactions may even lead to incommensurate magnetic ordering in bulk systems, for which a typical example is the long-wavelength helical order of Mn$_3$Sn [7].

Among transition metal diborides CrB$_2$ is another challenging example of an itinerant antiferromagnetic (AFM) metal possessing incommensurate magnetic ordering. It crystallizes in the hexagonal AlB$_2$ (or C32) crystal structure with space group P6/mmm [8], in which honeycomb layers of boron alternate with triangular chromium layers, see figure 1. The magnetic structure was determined experimentally by neutron scattering by Funahashi *et al* [9], revealing that the Cr moments order antiferromagnetically with an incommensurate spin spiral in the Cr planes with ordering vector $0.285 \times (2\pi)/(a/2)$ along the $\langle 110 \rangle$ direction, i.e. a fraction of 0.86 along the distance from Γ to K (the direction Λ), and with Néel temperature 88 K; this description has been extended by recent experiments [10], where the spin-wave spectrum was measured across a large $(\mathbf{q}, \omega)$-window. A detailed investigation

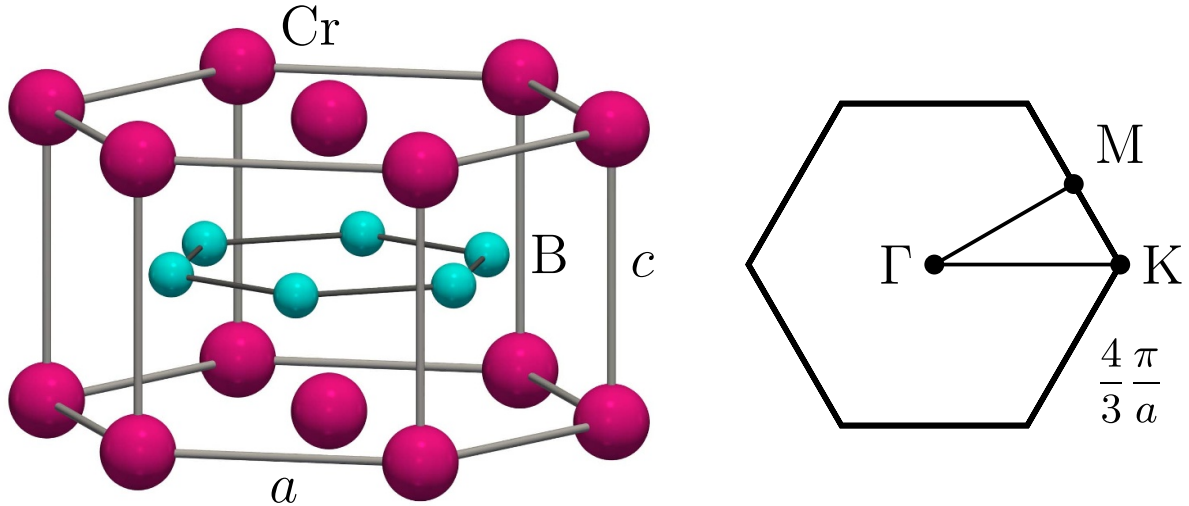* Author to whom any correspondence should be addressed.

Figure 1. Crystal structure of CrB$_2$. (Left) The direct lattice, where large (top and bottom layers) and small (middle layer) spheres denote Cr and B atoms, respectively. The lattice parameters a and c are also indicated. (Right) The hexagonal two-dimensional Brillouin zone for $q^z = 0$. Corresponding to C$_{3v}$ symmetry the irreducible wedge is bounded by the Γ–K–M triangle.

into the nature of magnetic ordering in CrB$_2$ was provided by Kaya *et al* [11], which confirmed that Cr moments form a simple helix structure, rotating in the plane formed by the c-axis and $\langle 110 \rangle$ (the propagation direction). An examination of the temperature-dependent conductivity of CrB$_2$ around the Néel temperature by Bauer *et al* [12] included the determination of the susceptibility, showing Curie–Weiss susceptibility with a large, negative Θ_{CW} indicative of strong frustration, together with a Cr moment of $\sim 2\,\mu_B$, in contrast to early neutron scattering experiments which indicated a Cr moment of $\sim 0.5\,\mu_B$ [9].

The electronic structure of CrB$_2$ has been examined theoretically in a number of works based on band theory using the local density approximation or generalized gradient approximation (GGA) for the exchange-correlation in density functional theory. Early calculations using non-self-consistent potentials [13] have been supplemented by linear muffin-tin orbital (LMTO) [14, 15] and later full-potential augmented plane-wave calculations. Of these more accurate GGA calculations, application of the generalized Bloch theorem (i.e. 'spin-spiral' calculations) showed ordering along $\mathbf{q} \approx 0.3\,\mathbf{q}_{110}$ and Cr moment $1.3\,\mu_B$ as part of detailed description of the de Haas–van Alphen effect [16].

The present work is aimed at extending our understanding of the magnetism in CrB$_2$ in terms of the Heisenberg exchange interactions leading to incommensurate ordering, both in the low-temperature limit, which we model as a ferromagnet (FM), and in the high-temperature limit where the local Cr moments are treated as fully disordered. First, we give brief details of the computational methods we used: the electronic structure calculations are based on Green's function (GF) multiple scattering formalism which facilitates the evaluation of magnetic exchange interactions and the study of the paramagnetic phase using the disordered local moment (DLM) method [17]. Then we present our results for the exchange interactions in both the FM and DLM states and give mean-field estimates for the wave vector $\mathbf{q}_0$ of the spin spiral

ground state and the Néel temperature T_N. These values are recalculated by spin dynamics and Monte Carlo simulations, respectively. We conclude that the DLM based spin models give more realistic description of the magnetism of CrB$_2$ than the spin model derived from the ordered (FM) state.

2. Details of calculations

Calculations have been performed using the screened Korringa–Kohn–Rostoker (SKKR) method [18] in the atomic-sphere approximation (ASA). The ASA describes the crystal potential by a sum of overlapping atomic spheres, neglecting the interstitial region; this approximation is appropriate for close-packed structures like AlB$_2$ materials including CrB$_2$. The ASA constraint, that the sum of sphere volumes equals the unit cell volume, does not determine the relative size of Cr and B spheres. We have experimented with sphere sizes obtained by minimizing the average sphere overlap and by scaling up touching spheres defined by the first maximum of the electrostatic potential and found that both configurations give closely similar results. For all calculations we assumed an in-plane lattice parameter of $a = 2.972$ Å and $c = 3.066$ Å according to experiments [8]. The resulting ASA radii are therefore $S_{Cr} = 1.580$ Å and $S_B = 0.929$ Å.

All calculations used an angular momentum cut-off of $\ell_{max} = 2$ and the GGA exchange-correlation parameterization as formulated by Perdew *et al* [19]. Sixteen energy points were used for complex contour integrations in energy, with 546 k-points in the two-dimensional Brillouin zone (2D BZ) for self-consistent-field calculations and up to 20 000 near the Fermi energy for computing exchange interactions. Ferromagnetic self-consistent calculations were combined with the relativistic torque method (RTM) to derive exchange interactions using infinitesimal rotations of the spins [20]. For the paramagnetic phase, the relativistic development of the DLM theory was used [17, 21], from which the adiabatic magnetic energy

surface was mapped onto a spin model using the spin-cluster expansion (SCE) [22].

The classical spin model we extract with the above methods is of the form

$$\mathcal{H} = -\frac{1}{2} \sum_{i \neq j} \mathbf{S}_i \underline{\underline{J}}_{ij} \mathbf{S}_j + \sum_i \mathbf{S}_i \underline{\underline{K}}_i \mathbf{S}_i, \qquad (1)$$

where i and j both run over all Cr atoms and $\mathbf{S}_i$ stands for classical spins of unit magnitude. Both the RTM and the SCE methods allow the extraction of the full $\underline{\underline{J}}_{ij}$ tensor, encompassing the isotropic exchange interaction, the Dzyaloshinskii–Moriya interaction and the two-site exchange anisotropy [20], the latter two ones originating from spin–orbit interaction. In the convention used in equation (1) a positive isotropic interaction corresponds to FM coupling. Note that the Dzyaloshinskii–Moriya interaction is absent due to inversion symmetry present between any two Cr atoms. The magnetic anisotropy is uniaxial, favouring out-of-plane Cr ordering. However, since the spin–orbit interaction is very weak in this system, the exchange anisotropy and the on-site anisotropy related to the matrix $\underline{\underline{K}}$ are also very small, in the order of $10\,\mu$Ry, and thus are not expected to significantly affect the ground state ordering.

We have repeated our calculations using the tight-binding LMTO GF method, as implemented in the Questaal code [23]. Compared with the SKKR calculations, the LMTO calculations use the same ASA construction, but were scalar-relativistic and used a 3rd order parameterization of the potential function, without inclusion of the combined correction for the potential overlap. Self-consistent LMTO-GF calculations involved integration on an elliptical energy contour with 35 points and a BZ mesh of $49 \times 49 \times 41$ points, by sampling. We found that the results of the two methods are in very good agreement.

The spin model of equation (1) has been studied using Monte Carlo and spin dynamics methods assuming classical statistics [24]. We used Landau–Lifshitz–Gilbert spin dynamics simulations at zero temperature as a means of energy minimization for a ground-state search. For this we first verified that the ground-state spin configuration has $q^z = 0$, then used a 64×64 Cr atom 2D lattice with free boundary conditions in-plane and periodic boundary condition perpendicular to the plane. Free boundary conditions are necessary in the plane in order not to impose spurious spatial modulation on a system that we expect to have incommensurate magnetic order, but the periodic boundary condition perpendicular to the plane allows us to restrict the phase space of the energy minimization to states that have $q^z = 0$. The simulations were converged in energy to below 10^{-8} Ry per Cr atom. For the temperature-dependence of the specific heat we used Metropolis Monte Carlo simulations on a $32 \times 32 \times 32$ Cr atom lattice with free boundary conditions in order to estimate the Néel temperature. The last 3×10^9 Monte Carlo time steps (corresponding to random single-spin flip attempts) were considered for thermal averaging out of 5×10^9 total time steps.

3. Results

First we performed self-consistent calculations by using the SKKR method in the FM and DLM states. For the FM state we obtained 1.564 μ_B spin moment for the Cr and 0.045 μ_B for the B atoms. In the DLM self-consistent calculation the Cr spin moment decreased to 1.344 μ_B, and there was no moment induced on the B sites due to the vanishing Weiss field in the paramagnetic state. This also justifies the softening of the Cr spin moment in the DLM state as compared to the FM state. LMTO (scalar-relativistic) Cr moments are 1.577 and 1.301 μ_B for the FM and DLM configurations, respectively. The FM spin moment is significantly larger than in earlier spin-spiral calculations of Brasse *et al* [16] which can be explained by the larger volume of the atomic sphere defining the atomic moment than the non-overlapping spheres used in full-potential methods.

We derived parameters for the spin model defined in equation (1) in terms of the SKKR method by using the RTM for the FM configuration and using the SCE for the DLM state. Within the scalar relativistic LMTO method the calculation of only the isotropic exchange interactions was possible by using the method of infinitesimal rotations [25, 26]. A comparison of the resulting isotropic Heisenberg couplings is shown in figure 2. The two magnetic reference configurations produce broadly similar spatial distributions of spin model parameters, with the two nearest neighbour (NN) shells visibly dominating the interaction landscape. In both cases the parameters obtained with SKKR and LMTO are in excellent agreement. The main feature we note is that the exchange couplings obtained using the FM reference are about twice as large as those for the DLM, which can partially be related to the larger magnitude of the Cr moment in the FM state. Though the first two NN shells correspond to almost the same interatomic distances, the respective interactions remarkably differ in size. This can be explained by the fact that the local neighbourhoods around the corresponding bonds are very distinct, e.g. the first NN bond is surrounded by four B atoms arranged in a rectangle, whereas the second NN bond goes through a ring of six B atoms.

With the definition in equation (1) in mind, it can be shown that the mean-field paramagnetic spin susceptibility can be related to the $\underline{\underline{J}}(\mathbf{q})$ lattice Fourier transform of the exchange tensors. In particular, the mean-field estimate predicts a magnetic ordering with highest critical temperature at the $\mathbf{q}_0$ wave vector for which the maximal eigenvalue $J(\mathbf{q})$ of the matrix $\underline{\underline{J}}(\mathbf{q})$ is the highest within the BZ; the corresponding ordering temperature is equal to $J(\mathbf{q}_0)/(3\,k_B)$. For a detailed derivation of this mean-field estimate see e.g. the appendix of [27].

The ordering wave vector from the mean-field estimates turned out in each case to lie along the Γ–K line connecting the centre of the hexagonal BZ with one of the vertices with $q_0^z = 0$. We have found that despite the apparent dominance of the first two FM NN couplings there is enough frustration in the system to push magnetic ordering away from the Γ point. The competition of these strong FM couplings with AFM further neighbours results in a delicate balance ultimately giving
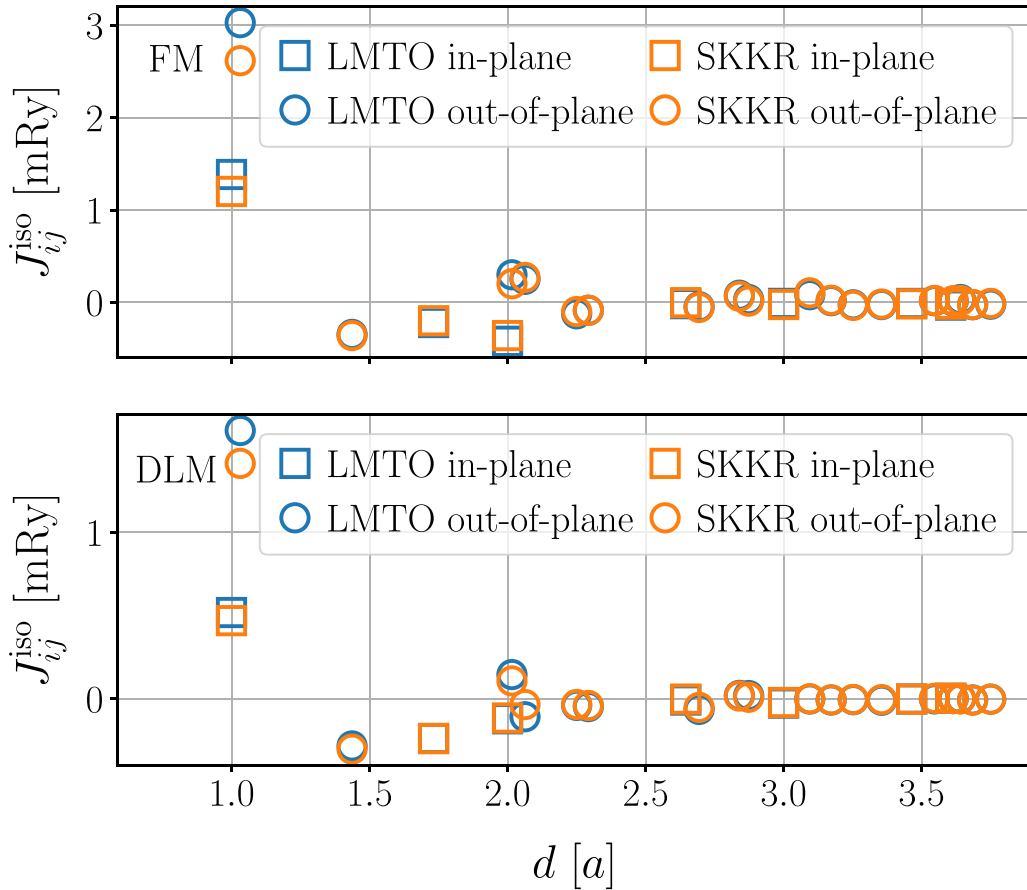
Figure 2. Isotropic Heisenberg couplings vs. interatomic distance. Parameters obtained with the SKKR (orange) and LMTO (blue) methods are compared for the FM (top) and DLM (bottom) reference states separately. Square and circle markers represent in-plane and out-of-plane neighbours, respectively.

rise to the incommensurate spin spiral ground state possessed by CrB_2.

In order to demonstrate this complex interplay of spin model parameters we computed the mean-field estimates while taking into consideration gradually more interacting neighbour shells. Figure 3 shows the dependence of the obtained mean-field ordering wave vectors as a function of this distance cut-off. Despite the magnitude of the first two NN couplings the mean-field theory shows that pairs as far as 2.8 lattice constant units (12 shells) are necessary to achieve convergence in the DLM state. This is even more so the case with the FM reference state, following the common observation that magnetic interactions tend to be shorter ranged in the DLM state due to spin disorder. We computed exchange interactions in the FM state via SKKR for up to nine lattice constant units to trace all distant interactions, and about $4.2\,a$ distance is necessary in order to achieve convergence. This extreme sensitivity to otherwise small exchange interactions is strong evidence for frustration.

We note that the sudden jumps in the mean-field q_0 estimate might first seem at odds with the fact that the corresponding distant interactions are small. However, these jumps are merely the result of small changes along a nearly degenerate line of the $J(\mathbf{q})$ function along the Γ–K line. When two local maxima of the function have a crossing (with respect to their

function values), the mean-field estimate for the ordering wave vector will abruptly jump from one maximum to the other. It is clear in the bottom of figure 3 presenting the mean-field Néel temperatures that there are no sudden changes beyond a cut-off of $2\,a$, where the last group of larger Heisenberg couplings are located.

The specific mean-field estimates are collected in table 1. Concerning the magnitude of the ordering vector there is some disagreement between the LMTO and SKKR calculations for the FM reference state. This can easily happen due to the delicate interplay of frustrated interactions we have demonstrated.

The $J(\mathbf{q})$ surfaces for these two spin models plotted in the entire 2D BZ in figure 4 reflect the frustrated nature of the exchange interactions. In both cases there is a nearly degenerate line along Γ–K, and this degeneracy is especially pronounced in case of the LMTO spin model. While the overall structure of the two surfaces is very similar, the numerical maximum is at an inner point of the Γ–K line for the SKKR couplings, whereas it is pushed out into the K point for the LMTO couplings. This is the reason for the difference in the mean-field ordering vectors seen in table 1.

Furthermore, considering the respective maximum $J(\mathbf{q})$ values, the mean-field Néel temperature is unreasonably high compared to experiments, even with accounting for the expected overestimation. Despite minor differences for some of the
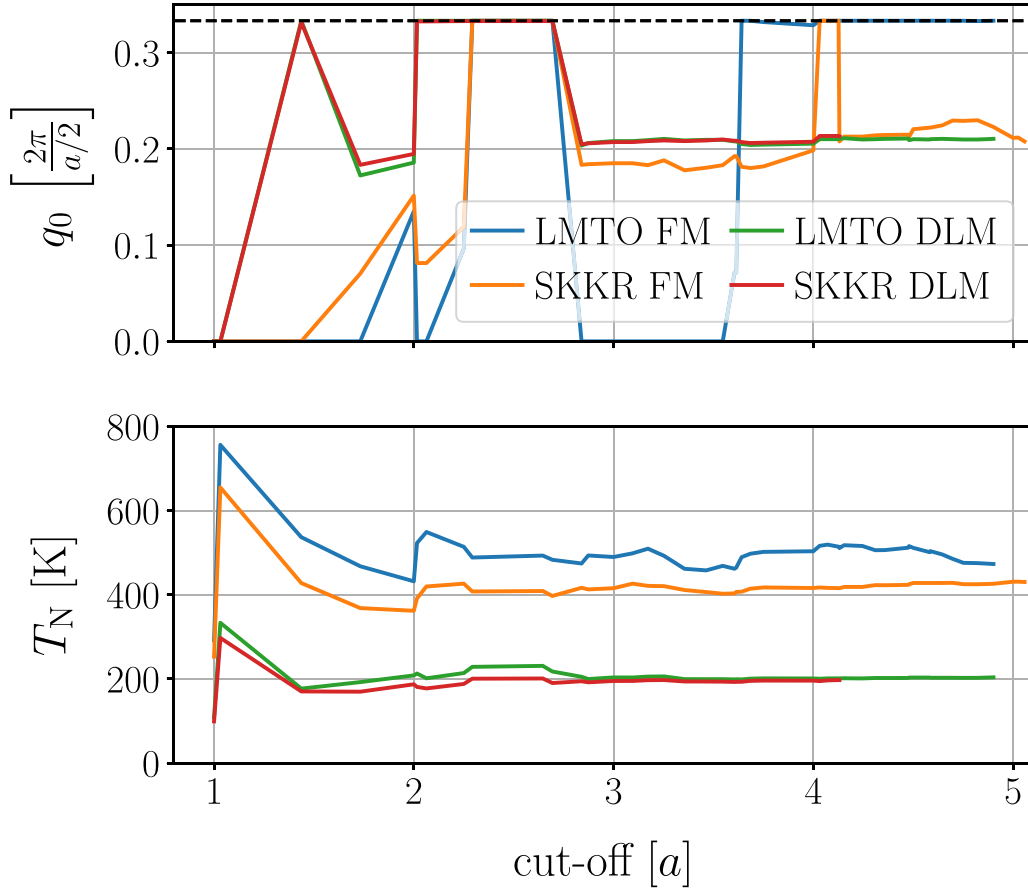
Figure 3. (Top) Magnitude of the mean-field ordering wave vector. $q = 0$ corresponds to the Γ point, whereas $q = \frac{1}{3} 2 \pi/(a/2)$, marked by the dashed line, corresponds to the K point of the BZ. (Bottom) Mean-field Néel temperature as a function of interatomic cut-off.
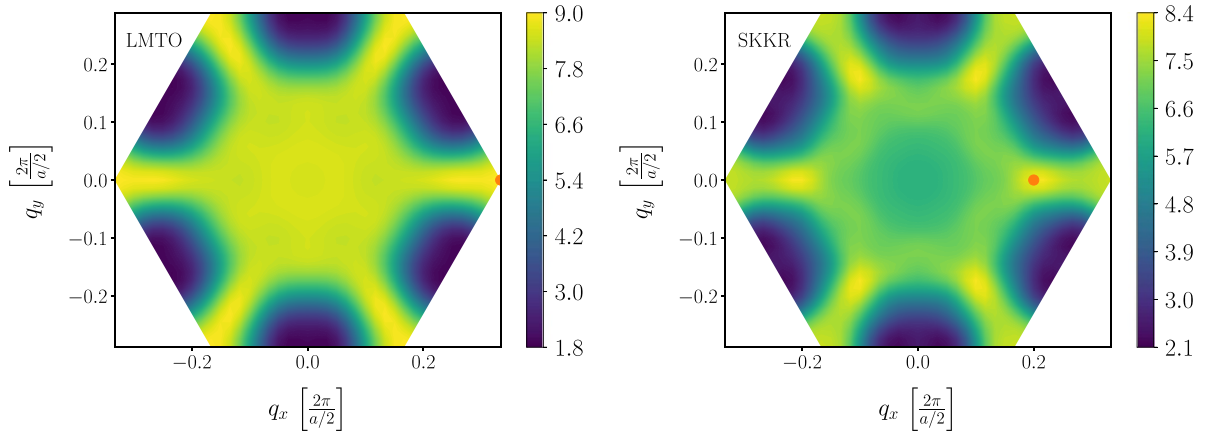

Figure 4. $J(\mathbf{q})$ surface for $q^z = 0$ in the 2D BZ for a FM reference state (left) using LMTO and (right) using SKKR-derived exchange interactions. The colourbars use mRy units. The vertices of the hexagonal 2D BZ (the K points) correspond to a triangular Néel state. The numerical maxima along a Γ–K line are indicated with orange circles.

largest exchange interactions derived in the DLM state, the mean-field value of the ordering vector is nearly the same in the two *ab initio* methods. Remarkably, the mean-field estimates for the Néel temperature from the DLM spin models are less than half of those from the FM spin models.

In order to verify the mean-field estimates and to obtain a realistic temperature scale we performed

Landau–Lifshitz–Gilbert spin dynamics simulations at zero temperature to find the ground-state spin configuration, and Monte Carlo simulations at finite temperature to locate the Néel transition. As shown in table 1, the spatial modulation of the ground state estimate from spin dynamics is in perfect agreement with the mean-field guess. With exception of the FM LMTO spin model, the magnitude of this wave vector of

Table 1. Estimates for the magnetic ordering. MF refers to the mean-field theory, while SD and MC refer to Landau–Lifshitz–Gilbert spin dynamics and Monte Carlo simulations, respectively. Calculated Néel temperatures are in K, ordering vectors are expressed in units of $2\pi/(a/2)$ along Γ–K (such that K is at 1/3). The Monte Carlo critical temperature is estimated from an inverse power-law fit to the peak of the specific heat from the left and right side, and the uncertainties are estimated from the disagreement between the temperatures obtained from the pair of fits for a given method. The experimental ordering vector occurs at $q_0^{\mathrm{exp}} = 0.285$; the experimental ordering temperature is 88 K [9].

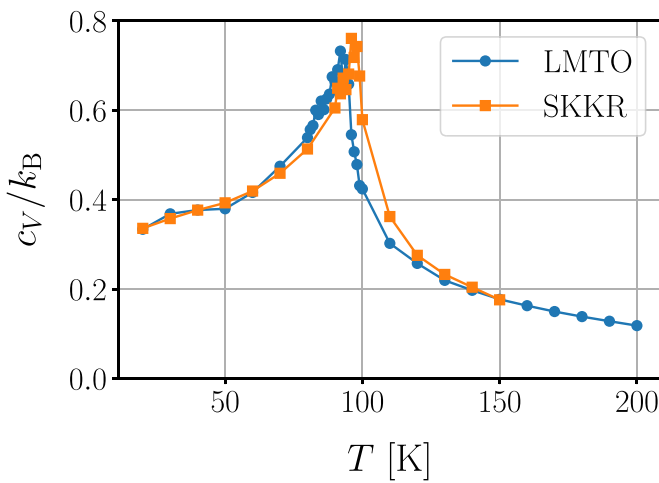| Reference	Method	q_0^{MF}	$T_{\mathrm{N}}^{\mathrm{MF}}$	q_0^{SD}	$T_{\mathrm{N}}^{\mathrm{MC}}$
FM	LMTO	0.333	475	0.330	187 ($\pm$3)
	SKKR	0.208	439	0.210	221 ($\pm$2)
DLM	LMTO	0.210	204	0.210	93 ($\pm$1)
	SKKR	0.213	197	0.213	97 ($\pm$1)

Figure 5. Specific heat in Boltzmann's constant units as a function of temperature obtained from Monte Carlo simulations in a system of $32 \times 32 \times 32$ spins.

about $0.21 \times (2\pi)/(a/2)$ is significantly smaller than seen in experiments and [16]. We attribute this inaccuracy to the significant frustration in this system; the combination of exchange interactions causing the spin-spiral ground state is quite delicate and depends sensitively on details of the theory, e.g. the exchange-correlation model. We note also that our calculations for the ordering vector are based on a bilinear spin model, missing higher-order multi-site exchange interactions, while methods based on total energy calculations, i.e. spin-spiral calculations [16], do not involve this restriction.

The temperature dependence of the specific heat from the Monte Carlo simulations of the DLM derived spin models is shown in figure 5. The sharp maximum of c_V clearly indicates the position of the transition temperature. The about 97 K Néel temperature we obtained is in good agreement with experimental findings. This agreement is not surprising since the DLM theory describes by construction the magnetic interactions at the critical temperature, whereas the exchange interactions derived by the torque method at the FM state are essentially to describe the low-temperature spin-wave spectra.

Indeed, the FM SKKR spin model resulted in a much too high Néel temperature of 221 K.

We note an interesting feature of our four spin models, namely that there is a striking 2.5 factor difference between the mean field estimate and the Monte Carlo result for the FM LMTO couplings, whereas for the other three spin models there is an almost exact factor of 2 instead. This dichotomy can probably be explained by the difference in ordered magnetic states: the triangular Néel structure (for the FM LMTO spin model) and a spin spiral with about 0.21 $2\pi/(a/2)$ wave number (for the other three spin models) may have different excitations, and thus significantly different fluctuations near the transition temperature.

4. Conclusions

In this work we presented Heisenberg exchange parameters describing the magnetism of CrB_2, which is known to have an incommensurate spin-spiral ground state. By modelling the system in the paramagnetic phase using the DLM theory as implemented in the SKKR and LMTO GF methods of density functional theory, we have reproduced the essential magnetic properties of the system without making any assumptions as to the nature of the magnetic ordering at lower temperature. In particular, the Néel temperature obtained with this theory is very close to that which is experimentally observed. The ordering direction is correctly reproduced by the spin model, but the wavelength of the ordering is underestimated. We demonstrate also that using the ferromagnetic state as reference results in significantly different exchange interactions which are substantially poorer than those derived in the paramagnetic phase. These conclusions are supported by rigorous testing with respect to the number of interacting shells of magnetic atoms.

Previous full-potential methods using the spin-spiral approach have found minimum energy configurations in better agreement with the experimental ordering vector [16]. This difference might be attributed either to the fundamental difference between our spin model based on mapping the band energy in the spirit of the force theorem [22, 25, 26] and the spin-spiral method based on total energy calculations or to the imprecision caused by the simplified representation of the Kohn–Sham potential in the ASA GF methods used here. In return for the modest loss of precision inherent in the ASA, the methods employed here allow a detailed mapping of the exchange interactions over many neighbour shells and highlight the complex frustration driving incommensurate ordering in this material. The resulting spin model correctly describes the thermodynamics of the spin system, despite the relatively small moment and small ordering temperature. It is possible that an improvement could be achieved by performing the RTM calculations with a non-collinear reference state that closely resembles the ground state of the system, however there is a strong debate still in the literature on the calculation of spin models from non-collinear reference states [28–31].

Data availability statement

The data that support the findings of this study are available upon reasonable request from the authors.

Acknowledgments

ORCID iDs

A Deák https://orcid.org/0000-0002-3210-2947
J Jackson https://orcid.org/0000-0002-2694-7038
B Nyári https://orcid.org/0000-0001-5524-9995
L Szunyogh https://orcid.org/0000-0001-7430-3627

References

[1] Lászlóffy A, Rózsa L, Palotás K, Udvardi L and Szunyogh L 2019 Magnetic structure of monatomic Fe chains on Re(0001): emergence of chiral multispin interactions *Phys. Rev.* B **99** 184430

[2] Lászlóffy A, Palotás K, Rózsa L and Szunyogh L 2021 Electronic and magnetic properties of building blocks of Mn and Fe atomic chains on Nb(110) *Nanomaterials* **11** 1933

[3] Rózsa L, Udvardi L, Szunyogh L and Szabó I A 2015 Magnetic phase diagram of an Fe monolayer on W(110) and Ta(110) surfaces based on *ab initio* calculations *Phys. Rev.* B **91** 144424

[4] Dupé B, Hoffmann M, Paillard C and Heinze S 2014 Tailoring magnetic skyrmions in ultra-thin transition metal films *Nat. Commun.* **5** 4030

[5] Dupé B, Bihlmayer G, Böttcher M, Blügel S and Heinze S 2016 Engineering skyrmions in transition-metal multilayers for spintronics *Nat. Commun.* **7** 11779

[6] Rózsa L, Deák A, Simon E, Yanes R, Udvardi L, Szunyogh L and Nowak U 2016 Skyrmions with attractive interactions in an ultrathin magnetic film *Phys. Rev. Lett.* **117** 157205

[7] Park P *et al* 2018 Magnetic excitations in non-collinear antiferromagnetic Weyl semimetal Mn_3Sn *npj Quantum Mater.* **3** 63

[8] Portnoi K I, Romashov V M and Romanovich I V 1969 Diagram of state of the chromium-boron system *Sov. Powder Metall. Met. Ceram.* **8** 298–302

[9] Funahashi S, Hamaguchi Y, Tanaka T and Bannai E 1977 Helical magnetic structure in CrB_2 *Solid State Commun.* **23** 859–62

[10] Park P *et al* 2020 Momentum-dependent magnon lifetime in the metallic noncollinear triangular antiferromagnet CrB_2 *Phys. Rev. Lett.* **125** 027202

[11] Kaya E, Kousaka Y, Kakurai K, Takeda M and Akimitsu J 2009 Spherical neutron polarimetry studies on the magnetic structure of single crystal $Cr_{1-x}Mo_xB_2$ ($x = 0$, 0.15) *Physica* B **404** 2524–6

[12] Bauer A, Regnat A, Blum C G F, Gottlieb-Schönmeyer S, Pedersen B, Meven M, Wurmehl S, Kuneš J and Pfleiderer C 2014 Low-temperature properties of single-crystal CrB_2 *Phys. Rev.* B **90** 064414

[13] Liu S H, Kopp L, England W B and Myron H W 1975 Energy bands, electronic properties and magnetic ordering of CrB_2 *Phys. Rev.* B **11** 3463–8

[14] Vajeeston P, Ravindran P, Ravi C and Asokamani1 R 2001 Electronic structure, bonding and ground-state properties of AlB_2-type transition-metal diborides *Phys. Rev.* B **63** 045115

[15] Grechnev G E, Fedorchenko A V, Logosha A V, Panfilov A S, Svechkarev I V, Filippov V B, Lyashchenko A B and Evdokimova A V 2009 Electronic structure and magnetic properties of transition metal diborides *J. Alloys Compd.* **481** 75–80

[16] Brasse M, Chioncel L, Kuneš J, Bauer A, Regnat A, Blum C G F, Wurmehl S, Pfleiderer C, Wilde M A and Grundler D 2013 de Haas-van Alphen effect and Fermi surface properties of single-crystal CrB_2 *Phys. Rev.* B **88** 155138

[17] Gyorffy B L, Pindor A J, Staunton J, Stocks G M and Winter H 1985 A first-principles theory of ferromagnetic phase transitions in metals *J. Phys. F: Met. Phys.* **15** 1337–86

[18] Zabloudil J, Hammerling R, Szunyogh L and Weinberger P 2005 *Electron Scattering in Solid Matter* (Berlin: Springer)

[19] Perdew J P, Burke K and Ernzerhof M 1996 Generalized gradient approximation made simple *Phys. Rev. Lett.* **77** 3865–8

[20] Udvardi L, Szunyogh L, Palotás K and Weinberger P 2003 First-principles relativistic study of spin waves in thin magnetic films *Phys. Rev.* B **68** 104436

[21] Staunton J B, Szunyogh L, Buruzs A, Gyorffy B L, Ostanin S and Udvardi L 2006 Temperature dependence of magnetic anisotropy: an *ab initio* approach *Phys. Rev.* B **74** 144411

[22] Szunyogh L, Udvardi L, Jackson J, Nowak U and Chantrell R 2011 Atomistic spin model based on a spin-cluster expansion technique: application to the $IrMn_3$/Co interface *Phys. Rev.* B **83** 024401

[23] Pashov D, Acharya S, Lambrecht W R L, Jackson J, Belashchenko K D, Chantis A, Jamet F and van Schilfgaarde M 2020 Questaal: a package of electronic structure methods based on the linear muffin-tin orbital technique *Comput. Phys. Commun.* **249** 107065

[24] Nowak U 2007 Classical spin models *Handbook of Magnetism and Advanced Magnetic Materials* (*Micromagnetism* vol 2) (New York: Wiley)

[25] Liechtenstein A I, Katsnelson M I, Antropov V P and Gubanov V A 1987 Local spin density functional approach to the theory of exchange interactions in ferromagnetic metals and alloys *J. Magn. Magn. Mater.* **67** 65–74

[26] Turek I, Kudrnovský J, Drchal V and Bruno P 2006 Exchange interactions, spin waves and transition temperatures in itinerant magnets *Phil. Mag.* **86** 1713–52

[27] Deák A, Szunyogh L and Ujfalussy B 2011 Thickness-dependent magnetic structure of ultrathin Fe/Ir(001) films: from spin-spiral states toward ferromagnetic order *Phys. Rev.* B **84** 224413

[28] Cardias R, Szilva A, Bezerra-Neto M M, Ribeiro M S, Bergman A, Kvashnin Y O, Fransson J, Klautau A B, Eriksson O and Nordström L 2020 First-principles Dzyaloshinskii–Moriya interaction in a non-collinear framework *Sci. Rep.* **10** 20339

[29] dos Santos Dias M, Brinker S, Lászlóffy A, Nyári B, Blügel S, Szunyogh L and Lounis S 2021 Proper and

improper chiral magnetic interactions *Phys. Rev.* B **103** L140408

[30] Cardias R *et al* 2022 Comment on "Proper and improper chiral magnetic interactions" *Phys. Rev.* B **105** 026401

[31] dos Santos Dias M, Brinker S, Lászlóffy A, Nyári B, Blügel S, Szunyogh L and Lounis S 2022 Reply to Comment on "Proper and improper chiral magnetic interactions" *Phys. Rev.* B **105** 026402

[32] Harris C R *et al* 2020 Array programming with NumPy *Nature* **585** 357

[33] Hunter J D 2007 Matplotlib: a 2D graphics environment *Comput. Sci. Eng.* **9** 90

[34] Guelton S, Brunet P, Amini M, Merlini A, Corbillon X and Raynaud A 2015 Pythran: enabling static optimization of scientific python programs *Comput. Sci. Discovery* **8** 014001

[35] Sullivan B and Kaszynski A 2019 PyVista: 3D plotting and mesh analysis through a streamlined interface for the Visualization Toolkit (VTK) *J. Open Source Softw.* **4** 1450